Histone deacetylase inhibitor belinostat regulates metabolic reprogramming in killing KRAS-mutant human lung cancer cells

Rebecca Mary Peter[a,b], **Md. Shahid Sarwar**[b], **Sarah Z. Mostafa**[b], **Yujue Wang**[c,d], **Xiaoyang Su**[c,d], **Ah-Ng Kong**[b,*]

[a]Graduate Program in Pharmaceutical Science, Ernest Mario School of Pharmacy, Rutgers, The State University of New Jersey, Piscataway, NJ 08854, USA

[b]Department of Pharmaceutics, Ernest Mario School of Pharmacy, Rutgers, The State University of New Jersey, Piscataway, NJ 08854, USA

[c]Metabolomics Shared Resource, Rutgers Cancer Institute of New Jersey, New Brunswick, NJ 08901, USA

[d]Department of Medicine, Rutgers-Robert Wood Johnson Medical School, New Brunswick, NJ 08901, USA

Abstract

Kirsten Rat Sarcoma virus (KRAS) oncogene, found in 20–25% of lung cancer patients, potentially regulates metabolic reprogramming and redox status during tumorigenesis. Histone deacetylase (HDAC) inhibitors have been investigated for treating KRAS-mutant lung cancer. In the current study, we investigate the effect of HDAC inhibitor (HDACi) belinostat at clinically relevant concentration on nuclear factor erythroid 2-related factor 2 (NRF2) and mitochondrial metabolism for the treatment of KRAS-mutant human lung cancer. LC-MS metabolomic study of belinostat on mitochondrial metabolism was performed in G12C KRAS-mutant H358 non-small cell lung cancer cells. Furthermore, L-methionine (methyl-^{13}C) isotope tracer was used to explore the effect of belinostat on one-carbon metabolism. Bioinformatic analyses of metabolomic data were performed to identify the pattern of significantly regulated metabolites. To study the effect of belinostat on redox signaling ARE-NRF2 pathway, luciferase reporter activity assay was done in stably transfected HepG2-C8 cells (containing pARE-TI-luciferase construct), followed by qPCR analysis of NRF2 and its target gene in H358 cells, which was further confirmed in G12S KRAS-mutant A549 cells. Metabolomic study reveals significantly altered metabolites related to redox homeostasis, including tricarboxylic acid (TCA) cycle metabolites (citrate, aconitate, fumarate, malate, and α-ketoglutarate); urea cycle metabolites (Arginine, ornithine, argino-succinate, aspartate, and fumarate); and antioxidative glutathione metabolism pathway (GSH/GSSG and NAD/NADH ratio) after belinostat treatment. ^{13}C stable isotope labeling data indicates potential role of belinostat in creatine biosynthesis via methylation of guanidinoacetate. Moreover, belinostat downregulated the expression of NRF2 and its target

*Correspondence to: Professor Ah-Ng Tony Kong, Department of Pharmaceutics, Ernest Mario School of Pharmacy, Rutgers, The State University of New Jersey, 160 Frelinghuysen Road, Piscataway, NJ 08854, USA. Voice: 848-445-6369/8; Fax: 732-445-3134; KongT@pharmacy.rutgers.edu.

Conflict of Interest

The authors declare no conflict of interest.

gene NAD(P)H:quinone oxidoreductase 1 (NQO1), indicating anticancer effect of belinostat is mediated, potentially via Nrf2-regulated glutathione pathway. Another HDACi panobinostat also showed potential anticancer effect in both H358 and A549 cells via Nrf2 pathway. In summary, belinostat is effective in killing KRAS-mutant human lung cancer cells by regulating mitochondrial metabolism which could be used as biomarkers for preclinical and clinical studies.

Graphical Abstract
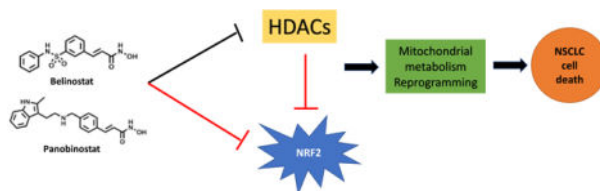
Keywords

HDAC inhibitor; Mitochondrial metabolism; KRAS mutation; NRF2; Lung cancer

1. Introduction

Histone deacetylases (HDACs) drive the expression of numerous genes and proteins involved in cancer development and progression. Inhibition of HDAC is an effective strategy for the treatment of cancer. Till now, eighteen HDACs have been identified from four different classes such as class I (HDACs 1, 2, 3, and 8), class IIA (HDACs 4, 5, 7, and 9), class IIB (HDACs 6 and 10), III HDACs (sirtuins 1–7) and class IV (HDAC11) (1, 2). Panobinostat, vorinostat, romidepsin, and belinostat are four HDAC inhibitors (HDACi) approved by the FDA for treating relapsed or refractory peripheral T-cell lymphoma. A wide body of literature reported that HDACi have shown the potential to overcome the therapeutic limitations of several drugs such as cyclin-dependent kinase (CDK) inhibitor seliciclib, tyrosine kinase inhibitor gefitinib, and mitogen-activated protein kinase kinase (also called MAP2K, MEK) inhibitor selumetinib (3). Belinostat (also known as PXD101), a novel hydroxamic acid pan-HDACi received FDA approval in 2014 for the treatment of T-cell lymphoma. Belinostat is being extensively investigated as monotherapy or with other anticancer agents to overcome drug resistance of cancer therapy (4–7). Belinostat or its derivatives contain N-hydroxycinnamamide bioactive fragment, which serves as both the zinc binding group and the linker group that possess very high HDAC binding affinity (8, 9), making these drugs promising in the treatment of various diseases, including cancer.

Lung cancer is the leading cause of cancer deaths in the US (10). There are two main subtypes, small cell lung cancer (SCLC) and non-small cell lung cancer (NSCLC). The latter accounts for over 80% of lung cancers. Although immense study is carried out in lung cancer research, the 5-year survival rate of lung cancer patients is limited to only 14%, necessitating new treatment strategies (11). During the last decade, a number of oncogenic drivers are described in NSCLC, namely Kirsten Rat Sarcoma viral oncogene (KRAS), Epidermal Growth Factor Receptor (EGFR), and Anaplastic Lymphoma Kinase (ALK), and each of them represent a potential therapeutic target. (12) The most frequently detected

KRAS mutations representing roughly 20–25% of NSCLC cases (13) are mutually exclusive to EGFR mutations and also a predictive indicator of resistance to chemotherapy and EGFR Tyrosine kinase inhibitor (TKI) (14, 15). Mutant KRAS is found to drive tumor growth by altering cancer cell metabolism, which influence tumor-microenvironment interactions and cancer progression (16, 17).

KRAS oncogenes mediate cellular and metabolic reprogramming during tumorigenesis by catalyzing glycolytic rate, decreasing oxidative flux via tricarboxylic acid (TCA) cycle, and enhancing glutamine metabolism to support cancer cell growth (18, 19). Emerging evidence suggest distinct metabolic profiles exist not just between KRAS wild type and KRAS-mutants, but also among different KRAS mutations, implying different responses to cancer therapies (20). Metabolic reprogramming is recognized as one of the hallmarks of cancer. Rewiring of cellular metabolism directly or indirectly influences oncogenic mutations, gene expression, and tumor microenvironment (21). The metabolic profile of lung cancer cells is defined by increased glucose uptake and glycolytic activity. Additionally, lung cancer cells exhibit significant alteration in metabolic pathways branching from glycolysis, such as pentose phosphate pathway (PPP), hexosamine biosynthetic pathway (HBP), serine-glycine pathway, and one-carbon metabolism (22).

Nuclear factor erythroid 2-related factor 2 (NRF2), a basic leucine zipper (bZIP) transcription factor, plays a critical role in the metabolic reprogramming of cancer. NRF2 is shown to cause inhibition of lipogenesis, facilitation of flux through the PPP, and increased nicotinamide adenine dinucleotide phosphate (NADPH) regeneration and purine biosynthesis via regulation of key metabolic enzymes or affecting the crosstalk with several oncogenic pathways (23, 24). NRF2 translocates from the Kelch-like ECH-associated protein1(KEAP1)-mediated ubiquitination and proteasomal degradation system and promotes normal cell survival by regulating the expression of antioxidant response element (ARE)–target genes. Nevertheless, it is suggested that there is also a "dark side of NRF2" (25). Prolonged activation of NRF2 causes the proliferation of cancer cells and promotes chemoresistance and radioresistance (25–29). A recent study observed enhanced glycosylation and glutaminolysis in early-stage lung cancer accompanied by NRF2 activation (30). Mutation of oncogenic KRAS proteins that regulate cell growth, differentiation, and apoptosis enhances the mRNA level of NRF2 via transcriptional activation of tetradecanoylphorbol-13-acetate response element situated in exon 1 of NRF2 (31). In addition, NRF2 promotes glutathione synthesis (GSH), which converts hydrogen peroxide to water via glutathione peroxidase enzyme. The oxidized GSH (GSSG) is reduced to GSH by utilizing NADPH, which may lead to the rewiring of cellular metabolism, including the tricarboxylic acid (TCA) cycle (32).

Although KRAS mutations were reported several decades ago, effective drugs that target KRAS-mutant proteins in advanced metastasized cancers are yet to be developed. No previous research has attempted to explore belinostat's metabolic effect in KRAS-mutant lung cancer with constitutive activation of NRF2. In this study, for the first time, we showed that clinically achievable concentration of belinostat has the capability to regulate metabolic perturbations in KRAS-mutant lung cancer.

2. Materials and methods

2.1. Chemicals and reagents

Roswell Park Memorial Institute (RPMI) 1640 medium, Dulbecco's modified Eagle's medium (DMEM), fetal bovine serum (FBS), penicillin-streptomycin (10000 U/ml), versene, and trypsin-ethylenediaminetetraacetic acid (EDTA) were purchased from Gibco. Dimethyl sulfoxide (DMSO) is supplied by Sigma-Aldrich. L-Methionine (Methyl-13C) was purchased from Cambridge Isotope Laboratories, Inc. (Andover, MA). Belinostat was supplied by Bepharm Scientific Inc. Panobinostat was purchased from Selleck, USA.

2.2. Cell culture

G12C KRAS-mutant H358 NSCLC cells were kindly provided by Dr. Sharon R Pine (Rutgers Cancer Institute of New Jersey). G12S KRAS-mutant A549 cells were obtained from Dr. Tamara Minko's lab (Rutgers University, NJ). H358 cells were cultured and maintained in RPMI 1640 supplemented with 10% FBS, 100 units/mL penicillin, and 100 μg/mL streptomycin at 37 °C in a humidified 5% CO_2 atmosphere. A549 cells were cultured and maintained in DMEM supplemented with 10% FBS, 100 units/mL penicillin, and 100 μg/mL streptomycin at 37 °C in a humidified 5% CO_2 atmosphere. HepG2 C8 cell line was established previously in our laboratory by transfecting human hepatocellular cells, HepG2 (obtained from ATCC) with pARE-TI-luciferase construct, provided by Dr. William Fahl, University of Wisconsin using a FuGENE™ 6 method (33). HepG2-C8 cells were cultured and maintained in DMEM supplemented with 10% FBS, 100 units/mL penicillin, and 100 μg/mL streptomycin at 37 °C in a humidified 5% CO_2 atmosphere.

2.3. Cell viability assay

MTS assay was used to determine the cell viability after treatment with belinostat or panobinostat, following the method of our published papers (34, 35). Briefly, H358, A549, and HepG2 C8 cells were seeded in 96-well plate at a density of 1×10^4 cells/well overnight to ensure cell adherence to the plate. The cells were treated with various concentrations of belinostat or panobinostat with 0.1% DMSO as negative control and incubated at 37 °C in a humidified, 5% CO_2 atmosphere for 24 h. Cell viability was determined using CellTiter 96® AQueous One Solution Cell Proliferation Assay System (Promega) at 490-nm absorbance as per the instructions provided by the manufacturer. Percentage of cell viability was calculated using the equation: absorbance of sample/absorbance of negative control×100. Three independent experiments were performed, and the data were plotted.

2.4. Apoptosis assay

Belinostat-induced apoptosis was determined at 1.25 and 80 μM in H358 cells using Alexa Fluor® 488 annexin V and propidium iodide (PI) staining (thermo fisher scientific). Briefly, H358 cells were incubated with belinostat for 24 h. After incubation, the cells were harvested and washed in cold phosphate-buffered saline. The washed cells were centrifuged and resuspended in 1X annexin-binding buffer. 100 μL of cell suspension (1 $\times 10^6$ cells/mL) was stained with 5 μL Alexa Fluor® 488 annexin V and 1 μL 100 μg/mL PI working solution. After the incubation period (15 mins) at room temperature, followed

by the addition of 400 μL 1X annexin binding buffer, stained cells were analyzed by flow cytometry (Beckman Coulter, Brea, CA).

2.5. LC-MS metabolomic analysis

The metabolomic profiling was performed by LC-MS method at the Metabolomic Shared Resources, Rutgers Cancer Institute of New Jersey, following the protocol of our recently published articles (34, 36). In brief, H358 cells were seeded overnight in 6-cm cell culture dish at a density of 1×10^6/dish. Next, cells were treated with 0.1% DMSO and 80 μM of belinostat for 3 and 24 h. Then, ice-cold extraction buffer composed of methanol, acetonitrile, and water at a ratio of 2:2:1 with 0.5% formic acid was used to extract metabolites from the cells. The volume of extraction buffer was adjusted in accordance with cell survival response to the treated dose to normalize the metabolite concentration. The samples were immediately placed on ice. After incubation for 5 min, the pH was adjusted by adding 50 μl 15% NH_4HCO_3. Cell extract was scraped from each dish, transferred to Eppendorf tube and centrifuged at 15,000 g for 10 min at 4°C. The supernatants containing the metabolites were separated and stored at −80°C until further analysis. Next, LC-MS analysis of the extracted metabolites was performed on a Q Exactive PLUS hybrid quadrupole-orbitrap mass spectrometer (ThermoFisher Scientific) coupled to hydrophilic interaction chromatography (HILIC). The LC separation was performed on Vanquish Horizon UHPLC system with an XBridge BEH Amide column (150 mm × 2.1 mm, 2.5 μM particle size, Waters) with the corresponding XP VanGuard Cartridge. To obtain the metabolite data MAVEN software was used.

2.6. ^{13}C Isotope labelling for metabolomic analysis

To further confirm the metabolic effect of belinostat, stable isotope tracer was introduced by preparing different concentrations of the drug in methionine-free RPMI medium supplemented with 2 mM L-methionine (methyl-^{13}C) as described previously (37–39). Briefly, 1×10^6 cells were seeded in a 6-cm cell culture dish overnight. The cells were then serum starved for 24 h followed by treatment with 0.1% DMSO and 80 μM belinostat for 3 and 24 h. Cell metabolites were then collected and analyzed by LC-MS, as described in the previous section.

2.7. Total RNA extraction and quantitative real-time PCR

Total RNA was extracted from H358 and A549 cells using GeneJET RNA Purification Kits (Thermo Fisher Scientific, Rockford, IL). RNA concentrations were measured using Infinite M200 PRO. About 500 ng of RNA was used for reverse transcription by Taqman Reverse Transcription Reagents (Thermo Fisher Scientific). The realtime PCR reactions were performed in triplicates with PowerUp SYBR Green Master Mix Kit (Thermo Fisher Scientific) on the QuantStudio 5 Real-Time PCR System (Thermo Fisher Scientific). The messenger RNA (mRNA) expression levels were quantified by the   Ct method and normalized against GAPDH levels. The primer sequences are as follows: GAPDH: 5'-GGTGTGAACCATGAGAAGTATGA-3' and 5'-GAG TCCTTCCACGATACCAAAG-3'; NRF2: 5'-TGATTCTGACTCCGGCATTT-3' and 5'-GCCAAGTAGTGTGTCTCCATAG-3'; NQO1: 5'- GGAAGAAACGCCTGGAGAATA-3' and 5'-AGAATCCTGCCTGGAAGTTTAG-3'.

2.8. Luciferase reporter activity assay

Stably transfected human hepatoma HepG2-C8 cells with pARE-TI-luciferase construct (40) were treated with belinostat to determine their effect on ARE-NRF2 pathway. Briefly, 1×10^5 HepG2-C8 cells per well were seeded in 12-well plate in 1 mL of cell culture medium, incubated overnight at 37°C in a humidified 5% CO_2 atmosphere and subjected to belinostat treatment (0.625, 1.25, 2.5, 5, 10 and 40 μM) for 24 h. 0.1% DMSO was used as the negative control. The cells were lysed using the reporter lysis buffer and 10 μL of the cell lysate supernatant was mixed with 50 μL of luciferase assay reagent (Promega) for analysis of luciferase activity using a Sirius luminometer (Berthold Detection System GmbH, Pforzheim, Germany) whose unit of measurement was relative luminous units per second (RLU/s). The reading obtained for each sample was normalized by protein concentration which was quantified using BCA protein assay (Pierce Biotech, Rockford, IL, USA). Luciferase activity was determined as a fraction of negative control.

2.9. Statistical analysis

2.9.1. Univariate analysis—Results are presented as mean ± standard error of the mean (SEM). Univariate data is analyzed using two-tailed t-test or one-way ANOVA corrected for multiple comparisons using Dunnett's test. P-value less than 0.05 was considered statistically significant. Each P value is adjusted for multiple comparisons.

2.9.2 Multivariate analysis

Principal component analysis (PCA): Principal Component Analysis (PCA) was used to investigate the influence of various metabolites under different conditions of study using GraphPad Prism version 9.0.2 for Windows, GraphPad Software, San Diego, California USA (www.graphpad.com). Since ionization rate (i.e. number of ions formed per molecule) of each identified metabolite may differ, metabolite intensities were standardized before performing PCA. Principal Components (PCs) were selected based on parallel analysis (Parallel analysis performs Monte Carlo simulations on "random" data of equal dimension to the input data and calculates eigenvalues for all resulting PCs). Percentile level to select PCs with eigenvalues greater than those from the simulations (number of simulations =1000) was chosen as 95%.

Hierarchical clustering analysis: To visualize the similarity of metabolite intensity expression levels across all treatment groups, hierarchical clustering analysis was performed using R software. After scaling the data and identifying optimal number of clusters (based on the average silhouette width for each k-value computed by k-means clustering algorithm), the result was represented using heatmap with the dendrogram. Pearson distance method was used to cluster the metabolite concentrations.

Enrichment pathway analysis: To detect biologically meaningful patterns that were potentially affected by significantly modulated metabolites by belinostat, metabolite set enrichment analysis (MSEA) was performed using MetaboAnalyst 5.0 against several libraries comprising ~9000 biologically meaningful metabolite sets collected mainly from human studies with more than 1500 chemical classes (41). Metabolites with absolute (PC1) score > 75% obtained from PCA analysis were used to identify the most enriched pathways.

3. Results

3.1. Cytotoxicity of belinostat and panobinostat in KRAS-mutant lung cancer cells

The cytotoxicity of belinostat and panobinostat against H358 and A549 cells was determined using MTS assay. Cell viability was reduced in a dose-dependent manner after 24 h treatment of belinostat (Fig. 1A) and panobinostat (Fig. 1B) in both cell lines. To examine the metabolic effects caused by belinostat in reducing cell survival rate of H358 cells, doses with cell survival rates around 50% (80 μM) were used for further experiments. Furthermore, the drug dose used in the study is clinically effective confirmed by the human pharmacokinetic studies of HDACi in cancer patients (6, 42, 43).

3.2. Belinostat induces apoptosis in H358 cells

To test the effect of 24 h treatment of belinostat on apoptosis of H358 cells, flow cytometry analysis was done after Alexa Fluor® 488 annexin V and propidium iodide (PI) staining. Clearly, the percentage of apoptosis showed a dose-dependent increase from 33.5 % at 1.25 μM dose to 61.41% at 80 μM dose (Fig. 1C). Apoptosis induced metabolic rewiring was studied by analyzing H358 cell-metabolites treated with 80 μM belinostat.

3.3. Belinostat regulates metabolic rewiring in H358 cells

Multivariate analyses were done on belinostat treated cell metabolites with respect to untreated condition. Based of PCA, the first two PCs explained 86.5% of the total variance in samples treated with belinostat with PC1 accounting for 77.67% of the overall variability, and 8.9% of total variability was described by PC2. The first component has been fairly effective in separating treatment groups based on time. Control group and belinostat-treated groups at 3 h are clustered together on the left side of zero line, indicating no significant change in the metabolite levels up to 3 h. However, a clear separation between control and 24 h treated groups indicated treatment effect of belinostat was most significant at 24 h (Fig. 2A). To determine the most enriched pathways after treatment of H358 cells with belinostat, metabolites with abs (PC1) loading score of 0.75 or more were used. Top 25 enriched pathways affected by belinostat were identified. Interestingly, belinostat was found to regulate metabolites of tricarboxylic acid (TCA)/citric acid (CAC) cycle and urea cycle (Fig. 2C). Among TCA cycle metabolites, belinostat increased the concentration of citrate, aconitate, isocitrate, alpha-ketoglutarate fumarate, and malate, with relative log2 fold change (with respect to control) increase of 3.4, 4.8, 3.4, 2.6, 2, and 3.2 folds, respectively (Fig. 3A). Also, belinostat upregulated concentrations of urea cycle metabolites, including arginino succinate, fumarate, arginine, and ornithine with relative log2 fold change (with respect to control) increase of 2.66, 2.03, 1.62, and 1.62 folds, respectively (Fig. 3B). Hierarchical cluster analysis helped to visualize alteration in metabolites, including amino acids at 24 h (Fig. 2B). Under the influence of belinostat, several amino acids, including phenylalanine, asparagine, methionine, tryptophan, and proline were upregulated with average log2(fold change) from 0.26 to 2.1 at 80 μM for 24 h (Fig. 4A). Additionally, belinostat altered the redox homeostasis of G12C KRAS-mutant H358 cells after 24 h by increasing ROS levels, which is evident from the decreased GSH/GSSG ratio, resulting in cell death. Treatment of 80 μM belinostat significantly lowered GSH/GSSG ratio by 61%. In addition, the cellular

NAD/NADH ratio was significantly decreased by more than 85% by belinostat, which clearly suggests modulation in the redox status of H358 cells (Fig. 4B).

3.4. Effect of belinostat on one-carbon metabolism in H358 cells

To get a complete view of one-carbon metabolism, an L-methionine (methyl-^{13}C) isotope tracer was used to trace S-adenosyl methionine (SAM), a co-factor in methylation of DNA CpG and histones with methyl group from methionine (44, 45). In the current study, ^{13}C methyl transfer was confirmed due to M+1 labeling in methionine and SAM. ^{13}C was further incorporated in creatine and creatine phosphate, which indicates potential role of belinostat in creatine biosynthesis via methylation of guanidinoacetate (Fig. 5A). Surprisingly, under untreated condition, most of the creatine was not labeled (>80%), which means SAM was not predominantly involved in creatine biosynthesis. After treatment with belinostat, SAM was driven to supply methyl group to synthesize creatine and creatine phosphate, as indicated by increased labeling of creatine and creatine phosphate (Fig. 5B). Overall, methylation potential was found to decrease after treatment with belinostat (Fig. 5C).

3.5. Belinostat and panobinostat inhibit constitutively activated NRF2

As evident from the metabolomic data showing modulation of GSH/GSSG and NAD/NADH ratio after belinostat treatment, we tested the effect of belinostat on NRF2 and its target gene NQO1 at the mRNA level. The results show that belinostat downregulated the expression of NRF2 and NQO1 by about 30% and 42%, respectively, in H358 cells. (Fig. 6A). The downregulation of NRF2 (32%) and NQO1 (54%) by belinostat was also confirmed in A549 cells (Fig. 6A). Furthermore, the effect of belinostat on ARE-NRF2 pathway was confirmed in stably transfected human hepatoma HepG2-C8 cell culture system (containing pARE-TI-luciferase construct) where belinostat inhibited ARE-NRF2 activity up to 40% at 40 μM dose (Fig. 6B). Additionally, panobinostat significantly downregulated NRF2 and NQO1 in A549 (by 58% and 81%, respectively) and H358 (by 37% and 66%, respectively) cells (Fig. 6C).

4. Discussion

For decades, it has been known that extensive metabolic rewiring occurs in cancer cells, and dysregulated metabolism causes resistance to cancer therapy (46, 47). A wide body of literature confirms targeting cancer metabolism is a promising strategy to overcome the resistance for the treatment of cancers (48, 49). HDAC inhibitors have been widely investigated for cancer treatments. Herein, for the first time, we investigated the metabolic activity of HDAC inhibitor belinostat in human KRAS-mutant lung cancer. Emerging evidence suggest that cancer cells, particularly those with mutated oncogenes and tumor suppressors rely on TCA cycle for energy production and synthesis of macromolecules such as nucleotides and lipids for cell growth advantages (50). Alterations in the TCA cycle imposed by dysfunction in cancer have been identified (51, 52). Citrate, the first intermediate of TCA cycle, is produced from oxaloacetate (OA) and acetyl-CoA in the presence of citrate synthase (CS). To maintain cell proliferation, hypoxic tumor cells tend to reverse the TCA cycle's flux by mediating the supply of cytosolic citrate to promote

lipogenesis (53). Our study suggests that belinostat causes upregulation of TCA cycle metabolites. Decreased concentration of citrate in cancer cells is an indicator of aggressive tumor growth (54). Hanai et. al. demonstrated that citrate accumulation caused increased apoptosis in mutant KRAS harboring NSCLC line (55). In our study, belinostat is found to increase citrate levels in KRAS-mutant H358 cells by 10-fold, which may lead to cell death (Fig 3A). Additionally, malate accumulation is observed during suppression of lung tumor growth (56), which could be an important biomarker for belinostat treatment as confirmed by Fig 3A.(57).

Recently, the urea cycle has been recognized as one of the most critical biochemical pathways in the study of NSCLC (58). But the role of urea cycle metabolites in promoting cell death has been explored in several other diseases. For instance, ornithine is shown to enhance AMPK autophagy to control tuberculosis infection (59). Also, the involvement of urea cycle metabolites in antitumor studies has been reported in colon (60) and breast cancer (61). Metabolic analysis of ^{13}C labeled metabolites suggests influence of belinostat in the creatine biosynthesis pathway. Creatine synthesis is an important component of arginine metabolism and arginine is one of the key metabolites of urea cycle. Therefore, the urea cycle is an important metabolic pathway regulated by belinostat, as observed in our study. Furthermore, amino acids are involved in pathways that feed cancer cells and provide building blocks for cancer cell growth (62). A study reveals KRAS-mediated metabolism causes alteration of metabolic pathways of the amino acids in KRAS-mutant clones as compared to cells lacking Ras pathway mutation. G12C KRAS-mutant clones have low levels of phenylalanine, methionine, asparagine, and proline compared with KRAS WT (20). Belinostat showed the potential to increase the concentration of these amino acids significantly.

Carcinoma reprograms nutrient acquisition and metabolism pathways to meet redox demands in cancer cells. Altered metabolism in cancer counteracts the metabolic effects of oncogene activation, tumor suppressor loss, and other stresses to maintain redox homeostasis (63). This includes constitutive upregulation of NRF2 and its target genes which continuously increase the capacity of cancer cells to scavenge ROS and promote cell proliferation (64). Cancer cells thus develop an antioxidant defense mechanism that regulates ROS levels needed for cancer initiation and transformation (65). Preclinical and clinical studies confirm that ROS modulates DNA damage response caused by chemotherapeutic drugs and ionizing radiation by mediating genotoxin-induced damage and oncogene-induced replication stress. Consequently, cells with DNA damage are subjected to cell cycle arrest (66). In the current study, the reduced ratio of GSH/GSSG and NAD/NADH may be implicated in increased oxidative stress either by induction of apoptosis or autophagy (67) caused by the clinically relevant concentration of belinostat potentially via NRF2 inhibition leading to cell death, which needs to be further validated. Interestingly, belinostat and panobinostat have shown the potential to inhibit NRF2 and its target gene NQO1, which qualifies it as a promising therapeutic drug in the treatment of NSCLC conferring constitutive activation of NRF2. Even though there is crosstalk between NRF2 and metabolic reprogramming during NSCLC development and progression (68), further investigation is required to understand the metabolic processes involved in NRF2 inhibition

and to measure the protein expression and cellular translocation of Nrf2 for the treatment of NSCLC.

5. Conclusion

In summary, for the first time, we have addressed the metabolic remodeling of KRAS-mutant lung cancer cells and NRF2 inhibition by HDAC inhibitors belinostat and panobinostat at their therapeutic concentration. Belinostat regulates the TCA cycle, urea cycle, glutathione, and amino acids metabolism, as well as inhibits NRF2 signaling to exert its overall anticancer effect. Thus, the anticancer potential of belinostat is exhibited through the ARE-NRF2 pathway and metabolic rewiring in lung cancer cells, making it a promising drug candidate for treating KRAS-mutant NSCLC.

Acknowledgments

Abbreviations:

ALK	Anaplastic lymphoma kinase
ARE	antioxidant response element
BEL	Belinostat
bZIP	basic leucine zipper
CDK	Cyclin dependent kinase
CS	citrate synthase
DMEM	Dulbecco's modified Eagle's medium
DMSO	Dimethyl sulfoxide
EDTA	ethylene diamine tetra acetic acid
EGFR	Epidermal growth factor receptor
ETC	electron transport chain
FBS	fetal bovine serum
HBP	hexosamine biosynthetic pathway
HDACs	Histone deacetylases
HDACi	HDAC inhibitors
KEAP1	Kelch-like ECH-associated protein1
KRAS	Kirsten rat sarcoma viral oncogene

MAP2K	mitogen-activated protein kinase kinase
mRNA	messenger RNA
MSEA	metabolite set enrichment analysis
NADPH	nicotinamide adenine dinucleotide phosphate
NQO1	NAD(P)H: quinone oxidoreductase 1
NRF2	Nuclear factor erythroid 2-related factor 2
NSCLC	Non-small cell lung cancer
OA	oxaloacetate
OGDH	2-oxoglutarate dehydrogenase
PCA	Principal component analysis
PI	propidium iodide
PPP	pentose phosphate pathway
RPMI	Roswell Park Memorial Institute
SCLC	small cell lung cancer
SEM	standard error mean
TCA	Tricarboxylic acid
TKI	Tyrosine kinase inhibitor
TRE	tetradecanoylphorbol-13-acetate (TPA) response element

References

1. Glozak MA, Seto E. Histone deacetylases and cancer. Oncogene. 2007;26(37):5420–32. Epub 2007/08/19. doi: 10.1038/sj.onc.1210610. [PubMed: 17694083]

2. Falkenberg KJ, Johnstone RW. Histone deacetylases and their inhibitors in cancer, neurological diseases and immune disorders (vol 13, pg 673, 2014). Nat Rev Drug Discov. 2015;14(3):219-. doi: 10.1038/nrd4579. [PubMed: 25656595]

3. Morelli MP, Tentler JJ, Kulikowski GN, Tan AC, Bradshaw-Pierce EL, Pitts TM, Brown AM, Nallapareddy S, Arcaroli JJ, Serkova NJ, Hidalgo M, Ciardiello F, Eckhardt SG. Preclinical Activity of the Rational Combination of Selumetinib (AZD6244) in Combination with Vorinostat in KRAS-Mutant Colorectal Cancer Models. Clin Cancer Res. 2012;18(4):1051–62. doi: 10.1158/1078-0432.Ccr-11-1507. [PubMed: 22173548]

4. Buckley MT, Yoon J, Yee H, Chiriboga L, Liebes L, Ara G, Qian X, Bajorin DF, Sun TT, Wu XR, Osman I. The histone deacetylase inhibitor belinostat (PXD101) suppresses bladder cancer cell growth in vitro and in vivo. J Transl Med. 2007;5:49. Epub 2007/10/16. doi: 10.1186/1479-5876-5-49. [PubMed: 17935615]

5. Zuo Y, Xu H, Chen Z, Xiong F, Zhang B, Chen K, Jiang H, Luo C, Zhang H. 17AAG synergizes with Belinostat to exhibit a negative effect on the proliferation and invasion of MDAMB231 breast cancer cells. Oncol Rep. 2020;43(6):1928–44. Epub 2020/04/03. doi: 10.3892/or.2020.7563. [PubMed: 32236631]

6. Abbott KL, Chaudhury CS, Chandran A, Vishveshwara S, Dvorak Z, Jiskrova E, Poulikova K, Vyhlidalova B, Mani S, Pondugula SR. Belinostat, at Its Clinically Relevant Concentrations, Inhibits Rifampicin-Induced CYP3A4 and MDR1 Gene Expression. Mol Pharmacol. 2019;95(3):324–34. Epub 2019/01/10. doi: 10.1124/mol.118.114587. [PubMed: 30622215]

7. Lobo J, Guimaraes-Teixeira C, Barros-Silva D, Miranda-Goncalves V, Camilo V, Guimaraes R, Cantante M, Braga I, Mauricio J, Oing C, Honecker F, Nettersheim D, Looijenga LH, Henrique R, Jeronimo C. Efficacy of HDAC Inhibitors Belinostat and Panobinostat against Cisplatin-Sensitive and Cisplatin-Resistant Testicular Germ Cell Tumors. Cancers (Basel). 2020;12(10). Epub 2020/10/15. doi: 10.3390/cancers12102903.

8. Zang J, Shi B, Liang X, Gao Q, Xu W, Zhang Y. Development of N-hydroxycinnamamide-based HDAC inhibitors with improved HDAC inhibitory activity and in vitro antitumor activity. Bioorg Med Chem. 2017;25(9):2666–75. Epub 2016/01/01. doi: 10.1016/j.bmc.2016.12.001. [PubMed: 28336407]

9. Rajak H, Singh A, Raghuwanshi K, Kumar R, Dewangan PK, Veerasamy R, Sharma PC, Dixit A, Mishra P. A structural insight into hydroxamic acid based histone deacetylase inhibitors for the presence of anticancer activity. Curr Med Chem. 2014;21(23):2642–64. Epub 2013/07/31. doi: 10.2174/09298673113209990191. [PubMed: 23895688]

10. Siegel RL, Miller KD, Jemal A. Cancer statistics, 2020. CA Cancer J Clin. 2020;70(1):7–30. Epub 2020/01/09. doi: 10.3322/caac.21590. [PubMed: 31912902]

11. Jiang ZB, Huang J, Xie C, Li X, Liu L, He J, Pan H, Huang L, Fan XX, Yao XJ, Xie Y, Li N, Liu L, He JX, Leung EL. Combined use of PI3K and MEK inhibitors synergistically inhibits lung cancer with EGFR and KRAS mutations. Oncol Rep. 2016;36(1):365–75. Epub 2016/04/29. doi: 10.3892/or.2016.4770. [PubMed: 27121230]

12. Lee T, Lee B, Choi YL, Han J, Ahn MJ, Um SW. Non-small Cell Lung Cancer with Concomitant EGFR, KRAS, and ALK Mutation: Clinicopathologic Features of 12 Cases. J Pathol Transl Med. 2016;50(3):197–203. Epub 2016/04/19. doi: 10.4132/jptm.2016.03.09. [PubMed: 27086595]

13. Addeo A, Banna GL, Friedlaender A. KRAS G12C Mutations in NSCLC: From Target to Resistance. Cancers (Basel). 2021;13(11). Epub 2021/06/03. doi: 10.3390/cancers13112541.

14. Eberhard DA, Johnson BE, Amler LC, Goddard AD, Heldens SL, Herbst RS, Ince WL, Janne PA, Januario T, Johnson DH, Klein P, Miller VA, Ostland MA, Ramies DA, Sebisanovic D, Stinson JA, Zhang YR, Seshagiri S, Hillan KJ. Mutations in the epidermal growth factor receptor and in KRAS are predictive and prognostic indicators in patients with non-small-cell lung cancer treated with chemotherapy alone and in combination with erlotinib. J Clin Oncol. 2005;23(25):5900–9. Epub 2005/07/27. doi: 10.1200/JCO.2005.02.857. [PubMed: 16043828]

15. Pao W, Wang TY, Riely GJ, Miller VA, Pan Q, Ladanyi M, Zakowski MF, Heelan RT, Kris MG, Varmus HE. KRAS mutations and primary resistance of lung adenocarcinomas to gefitinib or erlotinib. PLoS Med. 2005;2(1):e17. Epub 2005/02/08. doi: 10.1371/journal.pmed.0020017. [PubMed: 15696205]

16. Min HY, Lee HY. Oncogene-Driven Metabolic Alterations in Cancer. Biomol Ther (Seoul). 2018;26(1):45–56. Epub 2017/12/08. doi: 10.4062/biomolther.2017.211. [PubMed: 29212306]

17. Pupo E, Avanzato D, Middonti E, Bussolino F, Lanzetti L. KRAS-Driven Metabolic Rewiring Reveals Novel Actionable Targets in Cancer. Front Oncol. 2019;9:848. Epub 2019/09/24. doi: 10.3389/fonc.2019.00848. [PubMed: 31544066]

18. Racker E, Resnick RJ, Feldman R. Glycolysis and methylaminoisobutyrate uptake in rat-1 cells transfected with ras or myc oncogenes. Proc Natl Acad Sci U S A. 1985;82(11):3535–8. Epub 1985/06/01. doi: 10.1073/pnas.82.11.3535. [PubMed: 3858838]

19. Gaglio D, Metallo CM, Gameiro PA, Hiller K, Danna LS, Balestrieri C, Alberghina L, Stephanopoulos G, Chiaradonna F. Oncogenic K-Ras decouples glucose and glutamine metabolism to support cancer cell growth. Mol Syst Biol. 2011;7:523. Epub 2011/08/19. doi: 10.1038/msb.2011.56. [PubMed: 21847114]

20. Brunelli L, Caiola E, Marabese M, Broggini M, Pastorelli R. Capturing the metabolomic diversity of KRAS mutants in non-small-cell lung cancer cells. Oncotarget. 2014;5(13):4722–31. Epub 2014/06/24. doi: 10.18632/oncotarget.1958. [PubMed: 24952473]

21. Pavlova NN, Thompson CB. The Emerging Hallmarks of Cancer Metabolism. Cell Metab. 2016;23(1):27–47. Epub 2016/01/16. doi: 10.1016/j.cmet.2015.12.006. [PubMed: 26771115]

22. Vanhove K, Graulus GJ, Mesotten L, Thomeer M, Derveaux E, Noben JP, Guedens W, Adriaensens P. The Metabolic Landscape of Lung Cancer: New Insights in a Disturbed Glucose Metabolism. Front Oncol. 2019;9:1215. Epub 2019/12/06. doi: 10.3389/fonc.2019.01215. [PubMed: 31803611]

23. Chartoumpekis DV, Wakabayashi N, Kensler TW. Keap1/Nrf2 pathway in the frontiers of cancer and non-cancer cell metabolism. Biochem Soc Trans. 2015;43(4):639–44. Epub 2015/11/10. doi: 10.1042/BST20150049. [PubMed: 26551705]

24. Hayes JD, Dinkova-Kostova AT. The Nrf2 regulatory network provides an interface between redox and intermediary metabolism. Trends Biochem Sci. 2014;39(4):199–218. Epub 2014/03/22. doi: 10.1016/j.tibs.2014.02.002. [PubMed: 24647116]

25. Wang XJ, Sun Z, Villeneuve NF, Zhang S, Zhao F, Li Y, Chen W, Yi X, Zheng W, Wondrak GT, Wong PK, Zhang DD. Nrf2 enhances resistance of cancer cells to chemotherapeutic drugs, the dark side of Nrf2. Carcinogenesis. 2008;29(6):1235–43. doi: 10.1093/carcin/bgn095. [PubMed: 18413364]

26. Singh A, Misra V, Thimmulappa RK, Lee H, Ames S, Hoque MO, Herman JG, Baylin SB, Sidransky D, Gabrielson E, Brock MV, Biswal S. Dysfunctional KEAP1–NRF2 Interaction in Non-Small-Cell Lung Cancer. PLoS Med. 2006;3(10):e420. doi: 10.1371/journal.pmed.0030420. [PubMed: 17020408]

27. Jiang T, Chen N, Zhao F, Wang XJ, Kong B, Zheng W, Zhang DD. High levels of Nrf2 determine chemoresistance in type II endometrial cancer. Cancer Res. 2010;70(13):5486–96. Epub 2010/06/10. doi: 10.1158/0008-5472.Can-10-0713. [PubMed: 20530669]

28. Kim YR, Oh JE, Kim MS, Kang MR, Park SW, Han JY, Eom HS, Yoo NJ, Lee SH. Oncogenic NRF2 mutations in squamous cell carcinomas of oesophagus and skin. J Pathol. 2010;220(4):446–51. Epub 2009/12/08. doi: 10.1002/path.2653. [PubMed: 19967722]

29. Zhang P, Singh A, Yegnasubramanian S, Esopi D, Kombairaju P, Bodas M, Wu H, Bova SG, Biswal S. Loss of Kelch-like ECH-associated protein 1 function in prostate cancer cells causes chemoresistance and radioresistance and promotes tumor growth. Mol Cancer Ther. 2010;9(2):336–46. Epub 2010/02/04. doi: 10.1158/1535-7163.Mct-09-0589. [PubMed: 20124447]

30. Fahrmann JF, Grapov DD, Wanichthanarak K, DeFelice BC, Salemi MR, Rom WN, Gandara DR, Phinney BS, Fiehn O, Pass H, Miyamoto S. Integrated Metabolomics and Proteomics Highlight Altered Nicotinamide- and Polyamine Pathways in Lung Adenocarcinoma. Carcinogenesis. 2017;38(3):271–80. Epub 2017/01/05. doi: 10.1093/carcin/bgw205. [PubMed: 28049629]

31. Tao S, Wang S, Moghaddam SJ, Ooi A, Chapman E, Wong PK, Zhang DD. Oncogenic KRAS confers chemoresistance by upregulating NRF2. Cancer Res. 2014;74(24):7430–41. Epub 2014/10/24. doi: 10.1158/0008-5472.CAN-14-1439. [PubMed: 25339352]

32. Wang LJ, Wu RY, Sargsyan D, Su S, Kuo HC, Li SY, Chou PC, Sarwar MS, Phadnis A, Wang YJ, Su XY, Kong AN. Nfe2l2 Regulates Metabolic Rewiring and Epigenetic Reprogramming in Mediating Cancer Protective Effect by Fucoxanthin. Aaps J. 2022;24(1). doi: ARTN 30 10.1208/s12248-022-00679-0.

33. Yu R, Lei W, Mandlekar S, Weber MJ, Der CJ, Wu J, Kong ANT. Role of a Mitogen-activated Protein Kinase Pathway in the Induction of Phase II Detoxifying Enzymes by Chemicals1999;274(39):27545–52. doi: 10.1074/jbc.274.39.27545.

34. Hudlikar RR, Sargsyan D, Cheng D, Kuo HD, Wu R, Su X, Kong AN. Tobacco carcinogen 4-[Methyl(nitroso)amino]-1-(3-pyridinyl)-1-butanone (NNK) drives metabolic rewiring and epigenetic reprograming in A/J mice lung cancer model and prevention with Diallyl Sulphide (DAS). Carcinogenesis. 2021. Epub 2021/12/11. doi: 10.1093/carcin/bgab119.

35. Gao L, Cheng D, Yang J, Wu R, Li W, Kong AN. Sulforaphane epigenetically demethylates the CpG sites of the miR-9–3 promoter and reactivates miR-9–3 expression in human lung cancer A549 cells. J Nutr Biochem. 2018;56:109–15. Epub 2018/03/12. doi: 10.1016/j.jnutbio.2018.01.015. [PubMed: 29525530]

36. Li SY, Wu RY, Wang LJ, Kuo HCD, Sargsyan D, Zheng X, Wang YJ, Su XY, Kong AN. Triterpenoid ursolic acid drives metabolic rewiring and epigenetic reprogramming in treatment/prevention of human prostate cancer. Mol Carcinogen. 2022;61(1):111–21. doi: 10.1002/mc.23365.

37. Bott AJ, Shen J, Tonelli C, Zhan L, Sivaram N, Jiang YP, Yu X, Bhatt V, Chiles E, Zhong H, Maimouni S, Dai W, Velasquez S, Pan JA, Muthalagu N, Morton J, Anthony TG, Feng H, Lamers WH, Murphy DJ, Guo JY, Jin J, Crawford HC, Zhang L, White E, Lin RZ, Su X, Tuveson DA, Zong WX. Glutamine Anabolism Plays a Critical Role in Pancreatic Cancer by Coupling Carbon and Nitrogen Metabolism. Cell Rep. 2019;29(5):1287–98 e6. Epub 2019/10/31. doi: 10.1016/j.celrep.2019.09.056. [PubMed: 31665640]

38. Bianchi M, Crinelli R, Arbore V, Magnani M. Induction of ubiquitin C (UBC) gene transcription is mediated by HSF1: role of proteotoxic and oxidative stress. FEBS Open Bio. 2018;8(9):1471–85. Epub 2018/09/07. doi: 10.1002/2211-5463.12484.

39. Das S, Feng Q, Balasubramanian I, Lin X, Liu H, Pellon-Cardenas O, Yu S, Zhang X, Liu Y, Wei Z, Bonder EM, Verzi MP, Hsu W, Zhang L, Wang TC, Gao N. Colonic healing requires Wnt produced by epithelium as well as Tagln+ and Acta2+ stromal cells. Development. 2022;149(1). Epub 2021/12/16. doi: 10.1242/dev.199587.

40. Yu R, Mandlekar S, Lei W, Fahl WE, Tan TH, Kong AN. p38 mitogen-activated protein kinase negatively regulates the induction of phase II drug-metabolizing enzymes that detoxify carcinogens. J Biol Chem. 2000;275(4):2322–7. Epub 2000/01/25. doi: 10.1074/jbc.275.4.2322. [PubMed: 10644681]

41. Xia J, Wishart DS. MSEA: a web-based tool to identify biologically meaningful patterns in quantitative metabolomic data. Nucleic Acids Res. 2010;38(Web Server issue):W71–7. Epub 2010/05/12. doi: 10.1093/nar/gkq329. [PubMed: 20457745]

42. Bailey H, McPherson JP, Bailey EB, Werner TL, Gupta S, Batten J, Reddy G, Bhat G, Sharma S, Agarwal N. A phase I study to determine the pharmacokinetics and urinary excretion of belinostat and metabolites in patients with advanced solid tumors. Cancer Chemother Pharmacol. 2016;78(5):1059–71. Epub 2016/10/28. doi: 10.1007/s00280-016-3167-7. [PubMed: 27744565]

43. Liston DR, Davis M. Clinically Relevant Concentrations of Anticancer Drugs: A Guide for Nonclinical Studies. Clin Cancer Res. 2017;23(14):3489–98. Epub 2017/04/02. doi: 10.1158/1078-0432.CCR-16-3083. [PubMed: 28364015]

44. Jang C, Chen L, Rabinowitz JD. Metabolomics and Isotope Tracing. Cell. 2018;173(4):822–37. Epub 2018/05/05. doi: 10.1016/j.cell.2018.03.055. [PubMed: 29727671]

45. Zee BM, Levin RS, Xu B, LeRoy G, Wingreen NS, Garcia BA. In vivo residue-specific histone methylation dynamics. J Biol Chem. 2010;285(5):3341–50. Epub 2009/11/27. doi: 10.1074/jbc.M109.063784. [PubMed: 19940157]

46. Zhao Y, Butler EB, Tan M. Targeting cellular metabolism to improve cancer therapeutics. Cell Death Dis. 2013;4. doi: ARTN e532 10.1038/cddis.2013.60.

47. Locasale JW. Metabolic rewiring drives resistance to targeted cancer therapy. Mol Syst Biol. 2012;8. doi: ARTN 597 10.1038/msb.2012.30.

48. Galluzzi L, Kepp O, Vander Heiden MG, Kroemer G. Metabolic targets for cancer therapy. Nat Rev Drug Discov. 2013;12(11):829–46. doi: 10.1038/nrd4145. [PubMed: 24113830]

49. Nguyen TTT, Zhang YR, Shang EY, Shu C, Torrini C, Zhao JF, Bianchetti E, Mela A, Humala N, Mahajan A, Harmanci AO, Lei ZD, Maienschein-Cline M, Quinzii CM, Westhoff MA, Karpel-Massler G, Bruce JN, Canoll P, Siegelin MD. HDAC inhibitors elicit metabolic reprogramming by targeting super-enhancers in glioblastoma models. J Clin Invest. 2020;130(7):3699–716. doi: 10.1172/Jci129049. [PubMed: 32315286]

50. Anderson NM, Mucka P, Kern JG, Feng H. The emerging role and targetability of the TCA cycle in cancer metabolism. Protein Cell. 2018;9(2):216–37. Epub 2017/07/28. doi: 10.1007/s13238-017-0451-1. [PubMed: 28748451]

51. Scagliola A, Mainini F, Cardaci S. The Tricarboxylic Acid Cycle at the Crossroad Between Cancer and Immunity. Antioxid Redox Signal. 2020;32(12):834–52. Epub 2019/12/19. doi: 10.1089/ars.2019.7974. [PubMed: 31847530]

52. Eniafe J, Jiang S. The functional roles of TCA cycle metabolites in cancer. Oncogene. 2021;40(19):3351–63. Epub 2021/04/18. doi: 10.1038/s41388-020-01639-8. [PubMed: 33864000]

53. Filipp FV, Scott DA, Ronai ZA, Osterman AL, Smith JW. Reverse TCA cycle flux through isocitrate dehydrogenases 1 and 2 is required for lipogenesis in hypoxic melanoma

cells. Pigment Cell Melanoma Res. 2012;25(3):375–83. Epub 2012/03/01. doi: 10.1111/j.1755-148X.2012.00989.x. [PubMed: 22360810]

54. Icard P, Lincet H. The reduced concentration of citrate in cancer cells: An indicator of cancer aggressiveness and a possible therapeutic target. Drug Resist Updat. 2016;29:47–53. Epub 2016/12/04. doi: 10.1016/j.drup.2016.09.003. [PubMed: 27912843]

55. Hanai J, Doro N, Sasaki AT, Kobayashi S, Cantley LC, Seth P, Sukhatme VP. Inhibition of lung cancer growth: ATP citrate lyase knockdown and statin treatment leads to dual blockade of mitogen-activated protein kinase (MAPK) and phosphatidylinositol-3-kinase (PI3K)/AKT pathways. J Cell Physiol. 2012;227(4):1709–20. Epub 2011/06/21. doi: 10.1002/jcp.22895. [PubMed: 21688263]

56. Adam J, Hatipoglu E, O'Flaherty L, Ternette N, Sahgal N, Lockstone H, Baban D, Nye E, Stamp GW, Wolhuter K, Stevens M, Fischer R, Carmeliet P, Maxwell PH, Pugh CW, Frizzell N, Soga T, Kessler BM, El-Bahrawy M, Ratcliffe PJ, Pollard PJ. Renal cyst formation in Fh1-deficient mice is independent of the Hif/Phd pathway: roles for fumarate in KEAP1 succination and Nrf2 signaling. Cancer Cell. 2011;20(4):524–37. Epub 2011/10/22. doi: 10.1016/j.ccr.2011.09.006. [PubMed: 22014577]

57. Liu P, Wu D, Duan J, Xiao H, Zhou Y, Zhao L, Feng Y. NRF2 regulates the sensitivity of human NSCLC cells to cystine deprivation-induced ferroptosis via FOCAD-FAK signaling pathway. Redox Biol. 2020;37:101702. Epub 2020/09/09. doi: 10.1016/j.redox.2020.101702. [PubMed: 32898818]

58. Kim J, Hu Z, Cai L, Li K, Choi E, Faubert B, Bezwada D, Rodriguez-Canales J, Villalobos P, Lin YF, Ni M, Huffman KE, Girard L, Byers LA, Unsal-Kacmaz K, Pena CG, Heymach JV, Wauters E, Vansteenkiste J, Castrillon DH, Chen BPC, Wistuba I, Lambrechts D, Xu J, Minna JD, DeBerardinis RJ. CPS1 maintains pyrimidine pools and DNA synthesis in KRAS/LKB1-mutant lung cancer cells. Nature. 2017;546(7656):168–72. Epub 2017/05/26. doi: 10.1038/nature22359. [PubMed: 28538732]

59. Sivangala Thandi R, Radhakrishnan RK, Tripathi D, Paidipally P, Azad AK, Schlesinger LS, Samten B, Mulik S, Vankayalapati R. Ornithine-A urea cycle metabolite enhances autophagy and controls Mycobacterium tuberculosis infection. Nat Commun. 2020;11(1):3535. Epub 2020/07/17. doi: 10.1038/s41467-020-17310-5. [PubMed: 32669568]

60. Chen Y, Si L, Zhang J, Yu H, Liu X, Chen Y, Wu Y. Uncovering the antitumor effects and mechanisms of Shikonin against colon cancer on comprehensive analysis. Phytomedicine. 2021;82:153460. Epub 2021/01/22. doi: 10.1016/j.phymed.2021.153460. [PubMed: 33476976]

61. Huynh TYL, Oscilowska I, Saiz J, Niziol M, Baszanowska W, Barbas C, Palka J. Metformin Treatment or PRODH/POX-Knock out Similarly Induces Apoptosis by Reprograming of Amino Acid Metabolism, TCA, Urea Cycle and Pentose Phosphate Pathway in MCF-7 Breast Cancer Cells. Biomolecules. 2021;11(12). Epub 2021/12/25. doi: 10.3390/biom11121888.

62. Lieu EL, Nguyen T, Rhyne S, Kim J. Amino acids in cancer. Exp Mol Med. 2020;52(1):15–30. Epub 2020/01/26. doi: 10.1038/s12276-020-0375-3. [PubMed: 31980738]

63. Boroughs LK, DeBerardinis RJ. Metabolic pathways promoting cancer cell survival and growth. Nat Cell Biol. 2015;17(4):351–9. Epub 2015/03/17. doi: 10.1038/ncb3124. [PubMed: 25774832]

64. Klungland A, Robertson AB. Oxidized C5-methyl cytosine bases in DNA: 5-Hydroxymethylcytosine; 5-formylcytosine; and 5-carboxycytosine. Free Radic Biol Med. 2017;107:62–8. Epub 2016/11/29. doi: 10.1016/j.freeradbiomed.2016.11.038. [PubMed: 27890639]

65. Trachootham D, Alexandre J, Huang P. Targeting cancer cells by ROS-mediated mechanisms: a radical therapeutic approach? Nat Rev Drug Discov. 2009;8(7):579–91. Epub 2009/05/30. doi: 10.1038/nrd2803. [PubMed: 19478820]

66. Srinivas US, Tan BWQ, Vellayappan BA, Jeyasekharan AD. ROS and the DNA damage response in cancer. Redox Biol. 2019;25:101084. Epub 2019/01/08. doi: 10.1016/j.redox.2018.101084. [PubMed: 30612957]

67. Chen Y, McMillan-Ward E, Kong J, Israels SJ, Gibson SB. Oxidative stress induces autophagic cell death independent of apoptosis in transformed and cancer cells. Cell Death Differ. 2008;15(1):171–82. doi: 10.1038/sj.cdd.4402233. [PubMed: 17917680]

68. Zhao J, Lin X, Meng D, Zeng L, Zhuang R, Huang S, Lv W, Hu J. Nrf2 Mediates Metabolic Reprogramming in Non-Small Cell Lung Cancer. Front Oncol. 2020;10:578315. Epub 2020/12/17. doi: 10.3389/fonc.2020.578315. [PubMed: 33324555]
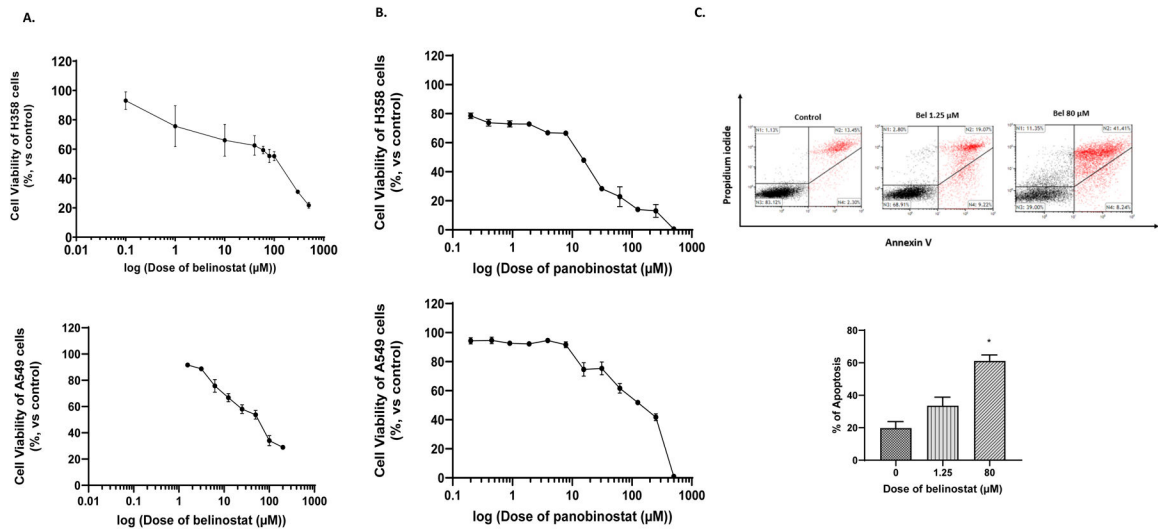
Fig. 1. Cytotoxic effect of belinostat and panobinostat in KRAS mutant lung cancer cells.
A. Cell viability in H358 and A549 cells after treatment with belinostat for 24 h. **B.** Cell viability in H358 and A549 cells after treatment with panobinostat for 24 h. **C.** Detection of apoptosis with Annexin-V and propidium iodide staining in H358 cells after treatment with belinostat for 24 h. % of apoptosis is expressed as mean ± SEM (n = 3). *p<0.05 compared with control.
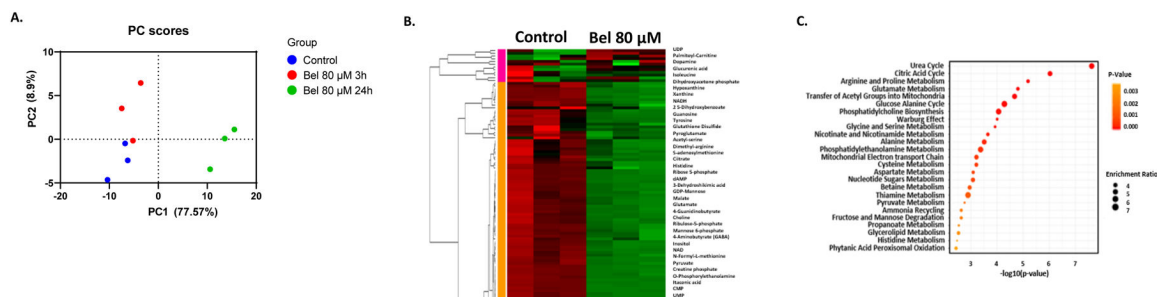
Fig. 2. Untargeted metabolomic analysis in H358 cells after treatment with belinostat for 24 h.
A. PCA analysis of metabolite sample data containing control group and treatment group at 3 and 24 h. **B.** Hierarchical cluster analysis of metabolite concentrations at 24 h. Color panel represents range of values determined by mean centering and scaling each row. **C.** Metabolite set enrichment analysis of metabolites that represent maximum variance i.e. absolute PC1 >0.75 among control group and treatment group at 24 h.
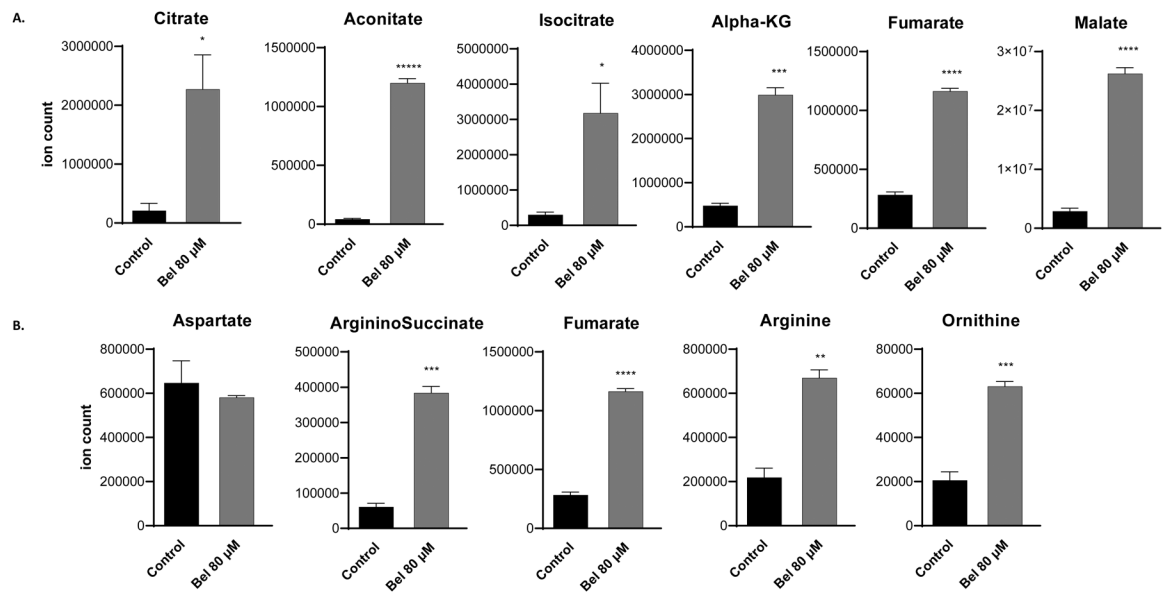
Fig. 3. Metabolic rewiring in H358 cells after treatment with belinostat for 24 h.
A. Regulation of TCA cycle metabolites. **B.** Regulation of urea cycle metabolites. Results are expressed as mean ± SEM (n = 3). *p < 0.05 compared with control.
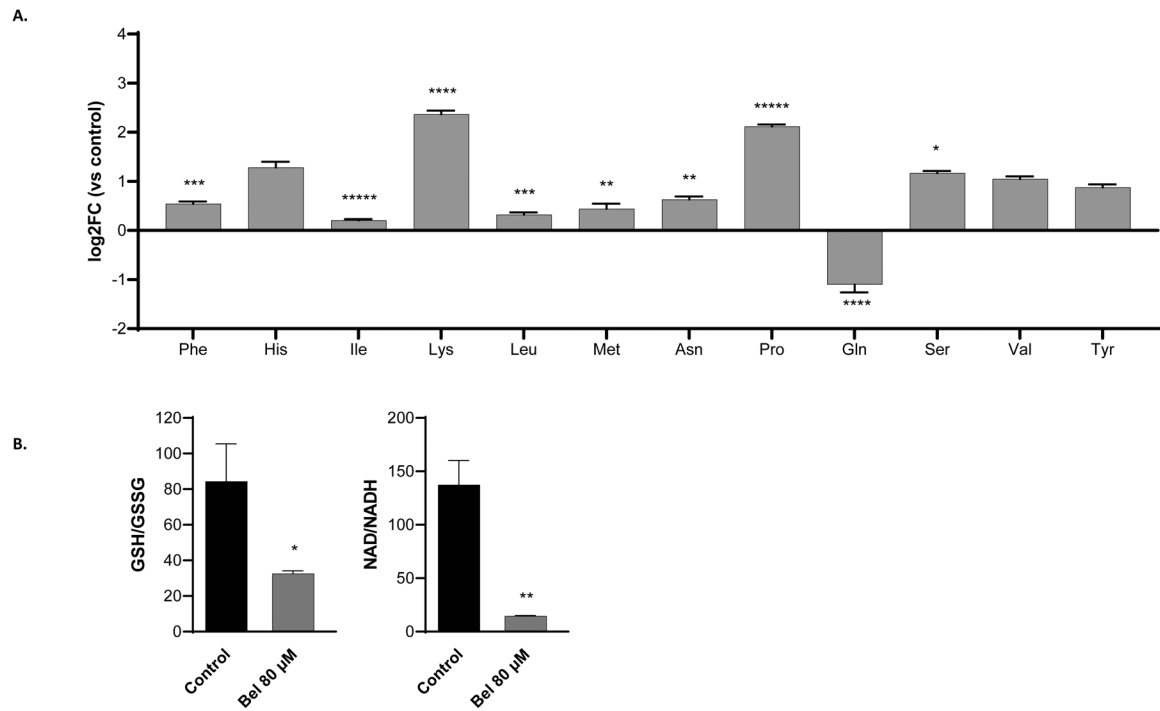
A.

B.

Fig. 4. Metabolic alteration of amino acids and redox status in H358 cells after treatment with belinostat for 24 h.

A. log2FC of amino acid concentrations relative to control after treatment with belinostat. **B.** Cellular redox state modulated by belinostat represented by GSH/GSSG and NAD/NADH. Results are expressed as mean ± SEM (n = 3). *p < 0.05 compared with control.
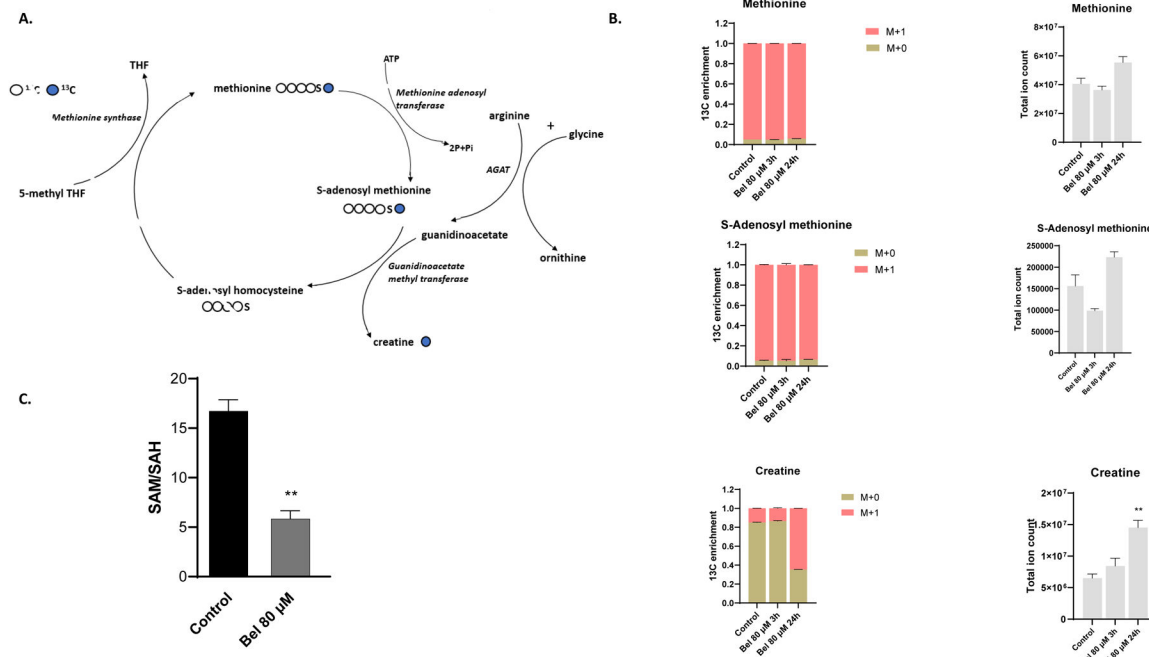
Fig. 5. Effect of belinostat on L-methionine (methyl-^{13}C) isotope tracer pathway in H358 cells after treatment with belinostat for 24 h.

A. Schematic representing proposed mechanism of action of L-methionine (methyl-^{13}C) isotope tracer after treatment with belinostat. **B.** ^{13}C enrichment and total ion count of labelled metabolites of creatine biosynthesis pathway. **C.** Methylation potential represented by SAM/SAH after treatment with belinostat. Result is expressed as mean ± SEM (n = 3). *p < 0.05 compared with control.
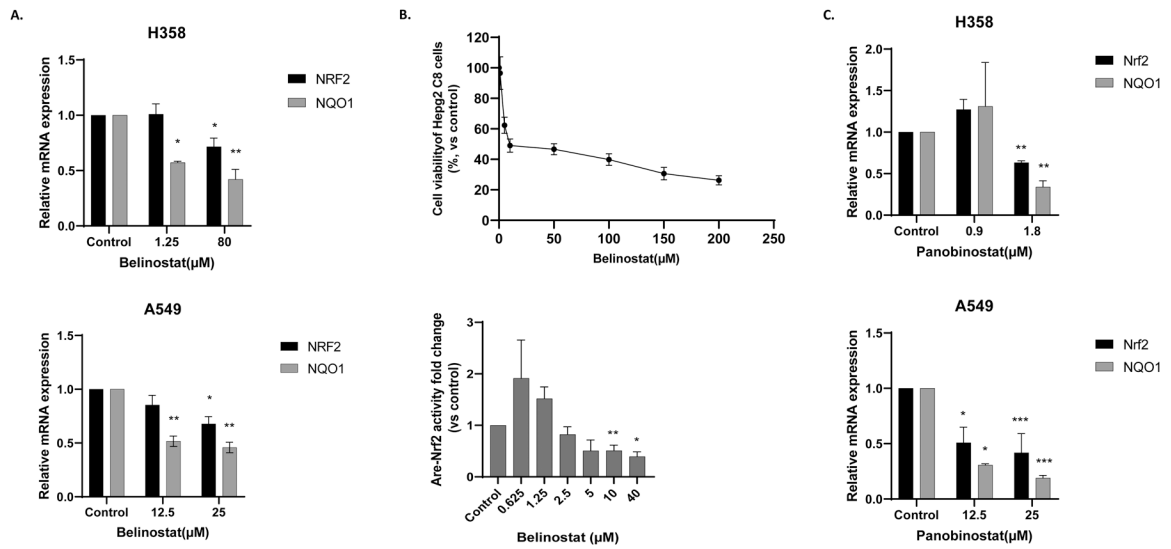
Fig. 6. Belinostat and panobinostat inhibit NRF2 signaling pathway.
A. RT-qPCR analysis of NRF2 and NQO1 in H358 and A549 cells after treatment with belinostat for 24 h. **B.** Effect of belinostat on cell viability and ARE-NRF2 pathway activity in HepG2 C8 cell culture system after 24 h treatment. **C.** RT-qPCR analysis of NRF2 and NQO1 in H358 and A549 cells after treatment with panobinostat for 24 h.